20

Local diffraction tomography of biological microobjects

© G.G. Levin[1], A.A. Samoilenko[1¶], I.V. Goryainova[1], G.V. Maksimov[2]

[1] All-Russian Research Institute for Optical and Physical Measurements, Moscow, Russia
[2] Lomonosov Moscow State University, Moscow, Russia

[¶] e-mail: asamoylenko@vniiofi.ru

Received June 20, 2025
Revised June 20, 2025
Accepted August 15, 2025

A method has been developed for using local tomography to study the morphology and dynamics of cells and subcellular structures, the propagation of optical radiation in which is described by the equations of diffraction tomography. It has been proven that the advantage of local tomography is that it is possible to quickly calculate the desired distribution at a point or region of interest of an object without conducting a complete reconstruction of the entire section, as well as to study biological cells whose size exceeds the field of view of the tomograph. An algorithm for detecting the coordinates of local density changes inside an object has been developed. Using mathematical modeling methods, an analysis of the sensitivity of local algorithms to changes within a cell model was performed, the parameters of which were chosen to be close to the characteristics of a native cell. Particular attention was paid to the comparison of local back-projection (Radon) and back-propagation (Devaney) algorithms for diffraction projections. The sensitivity of the algorithms to device phase noise and microscopic displacement of the object was studied for various observation time points. The results of experimental testing of the algorithms are presented using a set of local differential tomograms obtained during a study of changes in the leech Retzius neuron under the influence of the neurotransmitter glutamate. Measurements were performed on a differential tomograph over a 10-minute period. Analysis of the results showed that the developed method allows for the investigation of localized changes within the cell.

Keywords: diffraction tomography, local algorithms, living cell, dynamic density change.

DOI: 10.61011/EOS.2025.09.62311.8278-25

Introduction

Non-invasive investigation of the intracellular dynamics of the morphology of subcellular structures holds significant interest for both studying cell function and analyzing the effects of various substances on the cell. Currently, adequate approaches and methods are lacking for non-invasive studies that preserve the function of living cells, enabling measurements under *in vivo* and *in vitro* conditions on live, functioning biological objects. Meanwhile, challenges persist in directly observing subcellular systems, cell states, and the comprehensive dynamic changes in individual cells and their structures. It is evident that studying spatiotemporal changes in the cell using non-invasive methods will allow revealing the mechanisms of both cell state changes and the process of drug delivery into cells and individual cellular organelles.

Currently, computational tomography methods are widely used in optical phase microscopy to form a methodology for non-invasive measurement of the spatial distribution of the refractive index inside transparent objects, such as living cells [1–6]. It is evident that for studying three-dimensional changes in the cell cytoplasm, precisely the tomographic direction of phase and absorption microscopy can be used. This is due to the fact that obtaining projection data of the object is achieved by probing with a flat parallel light beam in various angular directions. In traditional tomography, the beam diameter must be larger than the object size. However, in practice, the size of the probing beam is often smaller than the area occupied by the object. In living cell microscopy, this may be due to the following reasons.

1. The need for high-resolution (magnification) investigation of the cell's subcellular organelles, at which the cell size becomes larger than the microscope's field of view.

2. The morphology and composition of cell biomolecules are specific, so the outer thin shell (plasma membrane and cytoskeleton) has a higher refractive index than the cytoplasm. This leads to light undergoing diffraction and/or refraction at the cell edges during optical probing. This effect can be eliminated by probing only the central part of the cell and using a light beam whose diameter is smaller than the transverse size of the cell.

3. The need to limit the investigation and probing area of the cell when studying the dynamics of individual internal organelles of the cell to reduce data acquisition time, minimize photodestruction of cell structures, and maintain overall cell functioning conditions.

We believe that for all the above tasks, the projection size should be smaller than the object size. Two main limitations can be identified that arise during the reconstruction of tomograms of such objects. First, the features of the optical scheme for multi-angle probing of cell preparations and cellular structures allow probing the object within a limited field of view [7]; second, such an object as, for example,

a nerve cell or a collection of cells exceeding the probing area leads to the problem of incomplete projections. These limitations make the task of reconstructing tomograms using inverse Radon transform or inversion of diffraction projections substantially ill-posed and lead to numerous artifacts in the reconstructed image, to compensate for which it is necessary to worsen the spatial resolution.

The necessity of reconstructing tomograms from spatially limited projections has led to the development of new algorithms and the emergence of so-called local tomography, which allows reconstructing tomograms only of those regions of the object that are of interest (Region-of-interest, ROI) [8,9]. Local tomography (or as it is sometimes called ROI-tomography) provides the possibility of independent and fast computation of the desired distribution at a point or region of interest without performing a full reconstruction.

Obviously, the images obtained in local tomography are only some approximation of the real density distributions inside the studied objects and require confirmation of the results using other methods (fluorescent microscopy, Raman spectroscopy, etc.). At the same time, the relationship between the distribution formed in local tomography and the true one is well known (see, for example, [10]). The main advantage of local tomography is its sensitivity to changes in the internal structure, which follows from the implementation of backprojection operations and summation of multi-angle projections. Therefore, it is of interest to use local tomography methods for analyzing changes occurring in the cell structure without performing its full three-dimensional reconstruction.

As is known, for living cells, several effects are characteristic that lead to changes in its phase image. First, local oscillations of the membrane, also called flicker, or dynamic fluctuations of the membrane. Second, movement of organelles inside the cell (cyclosis), third, changes associated with protein synthesis and decay, which lead to density fluctuations inside the cell. As a result of the indicated processes, changes occur in the phase of the light wavefront passed through the object. Importantly, local tomography allows detecting local changes in the internal structure of the cell, in particular, differentiating changes in the phase image of cell shape changes from density changes in both cytoplasm and subcellular structures. Also, it is possible to analyze the noise character, highlighting certain phase oscillation frequencies and assessing dynamic processes occurring in cells using them.

Previously, we identified features of local tomography based on Radon inversion and possibilities of its application for studying the internal structure of biological objects [10]. However, it is known that Radon inversion is valid only for the case when the propagation of radiation through the object is described either by the straight line equation or by a second-order curve. It is also possible to apply inverse transform for the case of single scattering in the Born or Rytov approximation for the eikonal equation [11,12]. At present, diffraction tomography methods based on this approximation are also used for studying living cells by optical tomography methods. Importantly, the possibility of applying local diffraction tomography (LDT) to biological objects has practically not been discussed.

The aim of this work was the development of LDT methods and investigation of their sensitivity to small changes in the internal structure of objects, to ensure measurements of local structural-morphological and dynamic characteristics of isolated functioning cells and cellular structures. An algorithm for determining the coordinates of the density change region inside a microobject is proposed, and special attention was paid to comparing diffraction and Radon local inversions applied to diffraction projections.

LDT Equations

To determine the main LDT equations, we limit ourselves to the two-dimensional case. Let the refractive index distribution inside the object be described by the function $f(x, y)$.

Following work [12], we write the diffraction projection equation as follows:

$$\overset{v}{f}_{\mathrm{D}}(p) \int_{-\infty}^{\infty} \frac{k_0}{\sqrt{k_0 - k^2}} \times \exp\left[-i\left[kp + \left(\sqrt{k_0^2 - k^2} - k_0\right)(q - l)\right]\right] \times dx dy \exp[ikp] dk, \quad (1)$$

where $k_0 = \frac{2\pi}{\lambda}$, φ — probing angle, $p = x\sin\varphi + y\sin\varphi$, $q = -x\sin\varphi + y\cos\varphi$, l — distance from the registration plane to the object center, k — coordinate in the frequency domain.

This equation was used for modeling the process of obtaining diffraction projections.

As the object, a mathematical model of a cell was taken, the size of which exceeds the field of view of the microscope. Its image is shown in Fig. 1, *a*.

Size of the image 256×256 pixels ($20 \times 20\,\mu$m). The object imitates a cell separated from the external environment by a flat membrane, with a nucleus and an inclusion of variable density. Immersion and liquid intracellular environment have equal refractive indices. The membrane and nucleus differ from the refractive index of the intracellular environment by Δn, equal to 0.1.

The calculation was performed in relative units, so the refractive index of immersion and intracellular environment is taken equal to zero: $n_{\mathrm{im}} = n_{\mathrm{icm}} = 0$, and the refractive indices of cellular structures (membrane, nucleus, inclusion) equal to $n_{\mathrm{cell}} = n_{\mathrm{icm}} + \Delta n = 0.1$.

Object shape. To imitate an extended cell whose size exceeds the field of view of the microobjective, the membrane represents two parallel lines at a distance $21\,\mu$m with thickness $1\,\mu$m and refractive index n_{cell}, equal to 0.1. The nucleus represents a circle located in the upper part of the

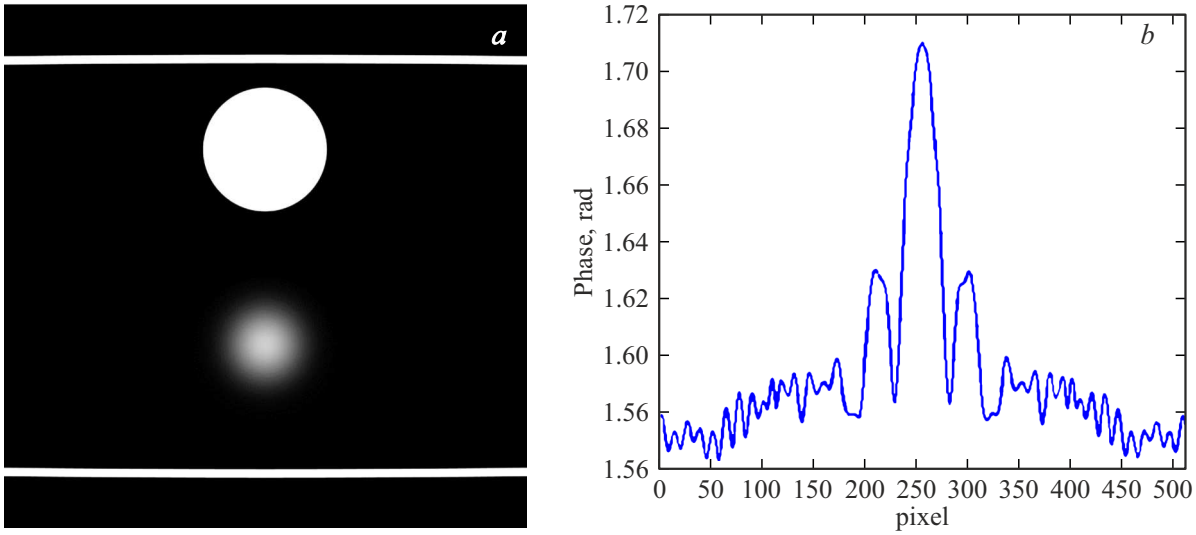

Figure 1. Model of cell section. (a) Diffraction projection of the model obtained at probing angle $\phi = 0$. (b) Projection computed according to formula (1).

cell, with diameter $4.8\,\mu$m and with uniformly distributed over the entire area of the circle refractive index n_{cell} equal in each point inside this circle to 0.1. The variable density inclusion represents a heterogeneity located in the lower part of the cell, with a refractive index distributed inside a circle of 30 pixels diameter according to the Gaussian law:

$$A \exp -\frac{(x - x_0)^2 + (y - y_0)^2}{\sigma^2},$$

where A is the maximum value of the Gaussian, equal to the refractive index $n_{\text{cell}} = 0.1$; x_0, y_0 -are the coordinates of the Gaussian center, and σ is the parameter defining the width of the Gaussian, $\sigma = 2.5\,\mu$m.

The object is illuminated by a plane wave from various directions. Fig. 1, b shows the central projection ($\varphi = 0$) computed from the model object.

Using the described model, a set of diffraction projections for different probing angles was formed.

The LDT algorithm is based on backpropagation equations [12]. In the case of limited projections, filtering required for tomogram reconstruction, as in diffraction or Radon tomography, is not possible [10]. Therefore, the formation of the diffraction sum image from limited projections can be described by the following expression

$$\overset{\text{V}}{f}_{\text{D}}(p, q) = \int_{-A}^{A} \overset{\text{V}}{f}_{\text{D}}(p') G(p - p', q - l) dp',$$

$$G(p, q) = \frac{1}{2\pi} \int_{-k}^{k} dk \exp i \left[kp + \left(\sqrt{k_0^2 - k^2} - k \right) q \right], \tag{2}$$

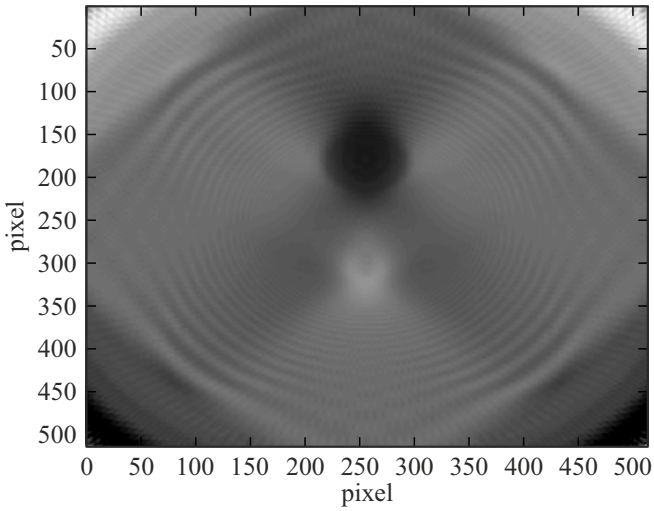

Figure 2. The reconstructed phase distribution image of the model cell Using the LDT algorithm with a limited probing angle ($\phi = \pm 37.5^\circ$) and apodized projections.

$$F_{\text{D}}(x, y) =$$

$$\int_{-\varphi_0}^{\varphi_0} \overset{\text{V}}{f}_{\text{D}}(x \sin\varphi + y \cos\varphi;\ -x \sin\varphi + y \cos\varphi,\ \varphi) d\varphi. \tag{3}$$

Further, a comparison is made of images obtained by local tomography reconstruction of diffraction projections for Devaney's (diffraction) and Radon's (linear) inversion formulas. The inversion formula for Radon local tomography is

$$F_{\text{R}}(x, y) = \int_{-\varphi_0}^{\varphi_0} \overset{\text{V}}{f}_{\text{D}}(x \sin\varphi + y \cos\varphi) d\varphi. \tag{4}$$

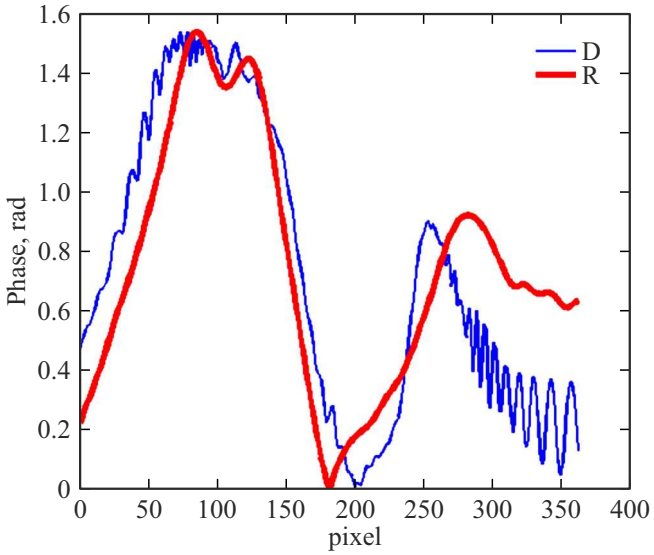

Figure 3. The distributions of the recovered phase corresponding to the density inside the cell (in relative units) calculated from diffraction projections of the model using the inverse projection algorithm (thick line, red curve) and the backpropagation algorithm (thin line, blue curve).

Sensitivity Analysis of LDT Method. Simulation

Application of local tomography methods in both diffraction and Radon approximations under limited angle and incomplete projections cannot reconstruct tomograms of acceptable quality. Therefore, it is necessary to limit the task and develop an algorithm for studying local internal cell dynamics, i.e., searching for coordinates of areas inside the cell with changes observed in its phase image or diffraction projection.

To study the effect of projection size limitation on local reconstruction quality, computer modeling was conducted for the cell model described previously. The projection size was artificially limited. It was found that limiting projection size in local reconstruction with backpropagation algorithms (formulas (2) and (3)) causes severe artifacts due to truncation function discontinuities at the projection edge. Edge effect compensation was performed by replacing all projection values above the „clipping“ line with an average computed along the chosen line, similarly for the lower clipping boundary. The restoration result from such halved sinogram is shown in Figure 2.

The study results indicate substantial image changes begin when projection sizes reduce to where backprojections no longer overlap the investigated change area. Therefore, in the further analysis of the sensitivity of the local reconstruction process to changes in the object, we limited ourselves to „clipped“ projections, where both inverse projection and backpropagation fully overlapped the selected region inside the object for all projections. In our case, this was the region inside the cell model where the inhomogeneity described by the Gaussian function is located.

It is important to exclude external factors affecting the object state and interference pattern (vibrations, optical element shifts, intrinsic phase noise) when studying cell dynamic changes. Micromovements during observations strongly affect reliable determination of changes' causes in phase images over time, critical, for example, in changing the cell incubation medium.

When analyzing the sensitivity of LDT, comparisons of the results from applying the backpropagation and inverse projection algorithms to diffraction projections are of interest, as such a comparison will reveal the characteristics of each algorithm and determine their areas of application.

When studying changes inside the cell, it is first necessary to select the region of changes, i.e., to determine the coordinates of the region where the refractive index (density) changes inside it along the depth (in the chosen direction) during the observation time.

The following algorithm was proposed and implemented [13], exemplified by the backprojection algorithm.

From phase images taken at angle $\varphi_0 = 0$ at time t_1 an area (x_1, y_1) is selected where fluctuations of shape or refractive index with coordinates $(z,\ x_1,\ y_1)$ are determined. When calculating the phase field distribution along the z axis using backpropagation, formulas (3) and (4) were used.

Figure 3 presents phase distribution restored values corresponding to cell density (arbitrary units) computed from diffraction projections by backprojection (R, red curve) and backpropagation (D, blue curve). The graph shows that the chosen backpropagation algorithm under limited projection and viewing angle results in minor diffraction oscillations (also visible in 2D image Figure 2). Maxima of inclusions inside the model shift relative to each other by several pixels. The maximum coordinate in the diffraction image is nearer the true heterogeneity position and has better resolution.

To detect density changes inside the cell, sums of phase values with the same (z, x_1, y_1) coordinates at time t_2 are computed, yielding function $f_2(z)$. The z value where the global extremum of difference $f_1(z) - f_2(z)$, occurs corresponds to the coordinate z within/on the cell surface where changes happen. Applying this algorithm across the entire set of n measurements determines phase sum changes over time related only to membrane shape deformation or density fluctuations in that cell area.

The instrument's phase noise on the difference between two images at different times will not depend on the coordinate z, as it will be compensated during subtraction and thus will not affect the coordinate of the global maximum, but will cause a constant shift of the entire distribution $f_1(z) - f_n(z)$. This constant component can easily be taken into account when analyzing the dynamics of object changes.

To investigate the sensitivity of various reconstruction methods to changes in the original object, the following simulation was conducted. The amplitude of the Gaussian

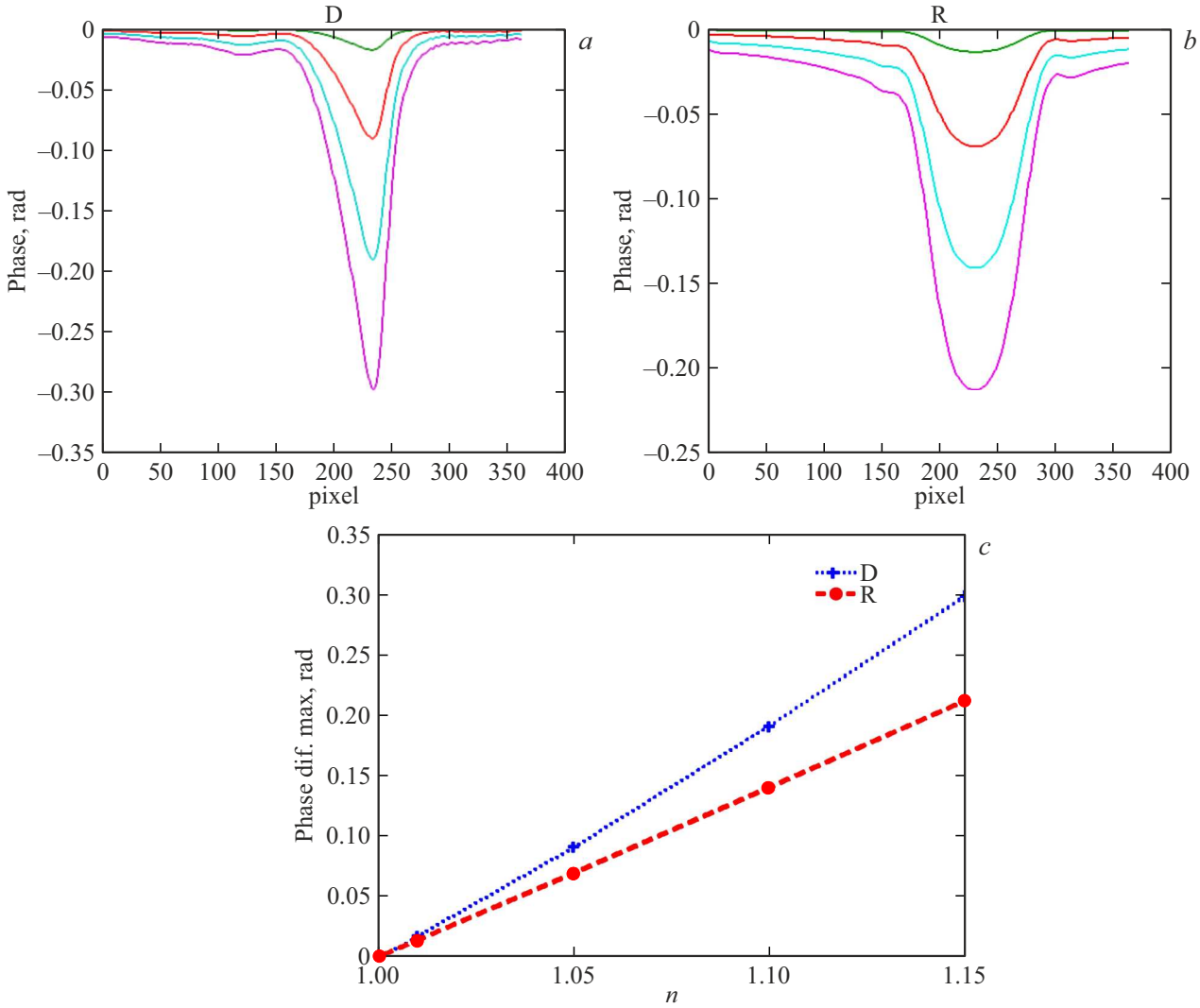

Figure 4. Differences in the phase distribution along the axis z calculated by the backpropagation method (D) for various amplitudes of the Gaussian function of the cell model (a). Differences in the phase distribution along the axis z calculated by the inverse projection method (R) for various amplitudes of the Gaussian function of the cell model (b). Graphs of the dependencies of the maxima of the phase difference distributions along the axis z on changes in the amplitude of the Gaussian function of the cell model (c).

function in the original object was changed by 2, 5, 10, and 15% of the initial value. In a number of works [14–16], it was shown that the refractive index of protein changes by exactly this amount during conformation. Diffraction projections were then calculated from the object using the developed algorithm. Each computed projection was „clipped“ by a factor of two, and the edges were apodized according to the algorithm described above. Local phase distributions along the selected direction parallel to the z-axis were then formed using inverse projection and backpropagation methods. The resulting two sets of four distributions each, corresponding to different amplitudes of the „Gaussian“ served as input data for determining the coordinates of the density change region inside the cell model. From each of these distributions, the first one with the minimum „Gaussian“ amplitude was subtracted.

Fig. 4, *a* shows the graphs corresponding to the recovery of the phase difference distribution along the axis z using the backpropagation method (D), for the case of probing angle change in the range $\pm 37.5^\circ$ and step between probing directions 4°. Such probing parameters were chosen because they correspond to the characteristics of the tomograph used in our experimental studies of large nerve cells [17].

In Fig. 4, *b*, similar distributions obtained by the inverse projection method (R) are presented. On the phase profiles, the coordinates of the inhomogeneity maximum do not coincide between different computation algorithms (Fig. 3), but on the phase difference distribution, the coordinates of the change maxima practically coincide with each other and with the inhomogeneity coordinates (Fig. 4, *a* and 4, *b*). The backpropagation algorithm provides higher resolution along the axis z and allows more accurate determination of the position of the changing inhomogeneity. Note that

small changes in probing angle and number of projections do not lead to any significant changes in the modeling results.

The presented curves describe not the recovered phase itself, but its variation with changes in the inhomogeneity amplitude on the model. For quantitative assessment of changes, graphs of the dependencies of the maxima of the distributions on Fig. 4, *a* and 4, *b*, from the parameter n which corresponds to the change in Gaussian amplitude on the model, were plotted. Along the ordinate axis on the picture below, phase values normalized to the Gaussian height are plotted, along the abscissa axis — the values of the parameter n. The parameter n equal to 1 corresponds to the initial (minimum) Gaussian amplitude. The value 1.15 corresponds to a 15% increase. From the graph, it follows that the dependence is linear for both algorithms, but backpropagation is more sensitive to object changes.

The proposed algorithm compensates for the instrument's own phase noises, but the influence of the live micro-object's own motion on the phase image change remains. Motions of the micro-object exceeding the micro-objective's resolution interval are noticeable on the phase image and can be compensated during subsequent processing. Small object oscillations within the resolution can affect the comparison of measurement results at different times. For our model, such micro-displacements correspond to 1−5pixels in the projection images.

In Fig. 6, the difference of two recovered phase distributions along the axis z passing through the inhomogeneity maximum is shown for different „Gaussian" amplitudes.

The obtained results of the proposed model indicate that reconstruction using inverse projection is little sensitive to small object displacements. In Fig. 6, *a*, the displacement of the second frame was one pixel, on Fig. 6, *b* — 3 pixels. When using the backpropagation algorithm, numerous false maxima arise, caused by the displacement of diffraction petals in the reconstructed image. This allows proposing a method for finding the coordinates of cell structure changes based on joint processing of images formed by different local reconstruction algorithms.

Experimental Validation of the LDT Method

In this series of experiments, the applicability of the algorithms described in the previous section to analyzing a real live micro-object — a neuron — was investigated. Retzius neurons of the leech [17] were used as the research object. The leech was kept for 60 min in a medium with 5-hydroxytryptophan (serotonin precursor), then the leech neuron was isolated and incubated in a medium containing 115 mmol NaCl, 4 mmol KCl, 1.8 mmol $MgCl_2$, 1 mmol $CaCl_2$, 10 mmol Tris, 10 mmol glucose. Since the cell size exceeded the microtome field of view, the selected projection size was smaller than the object. The cell thickness did not exceed $5-7\,\mu$m. During the experiment, neuron projections were first recorded in control, then in the experiment after injecting the neurotransmitter — glutamate — into the solution. The following series of experiments were conducted: control measurement (without glutamate addition), measurement with glutamate addition at concentration $5 \cdot 10^{-4}$ mmol/l and10^{-2} mmol/l to the cell. Tomogram changes were detected in the perimembrane area and perinuclear area of the cell (as vesicle clusters containing serotonin are localized there) only upon addition of 10^{-2} mmol/l glutamate. Measurements were performed after adding the active substance of high concentration to the sample. Tomogram reconstruction was performed from experimental data obtained on the neuron. Since the cell thickness is small and the phase shift is minor, differential projections were used for better visualization: over 10 min, data for 37 tomograms of 100 projections each were recorded, obtained in the angle range from $-32°$ to $32°°$.

For the experimental studies, an optical phase microtomo graph developed at VNIIMETP was used. Its scheme and design features are described in detail in [18,19]. ts basis is a transmission microscope with a lateral shift interferometer, which allows forming differential projections. As the source of low-coherence radiation, a point LED (Fig. 3) from Kyosemi Co., Japan, model KED080RAXH, was used, with central emission wavelength 652 nm, spectral half-width 10 nm, emission power 0.6 mW at current 25 mA with emitting area about $80\,\mu$m. The LED emission was collimated by an objective with focal length 12 mm. The sample was illuminated by a parallel light beam (at different angles) through a wide-aperture objective (100×, NA 1.30, immersion, UPlanFLN100X02, Olympus). For angular probing of the object, a scanner in the form of a uniaxial galvanometric mirror GVS011 (ThorLabs, USA) was used. The scanning angular range in this experiment was from $-32°$ to $32°$. The image was formed by the same objective used for illumination. Phase images were recovered by phase-step interferometry.

The obtained series of tomograms was processed according to the algorithm described in the previous sections. In Fig. 6, a differential projection obtained at $\varphi = 0$ for the first tomogram is presented. A point of interest in the perinuclear area of the cell where changes were observed was selected on it, marked with a circle on Fig. 6, *a* In Fig. 6, *b*, the time dependence of the phase change on the projection obtained at $\varphi = 0$in the selected point of interest is shown. Then, for each tomogram, the density distribution along the line parallel to the optical axis (axis z) containing the point of interest was recovered.

The distribution reconstruction was performed in the micro-objective focusing area during projection recording ($l = 0$ formula (1)). Tomogram analysis showed that only the central layer a few microns thick carries useful information. Therefore, density dependencies on time (tomogram number) were selected only for z in the range from-2 to $+2\,\mu$m. For convenience of comparison and compensation of microtomo graph phase noise, which is inevitable during a ten-minute experiment, the following

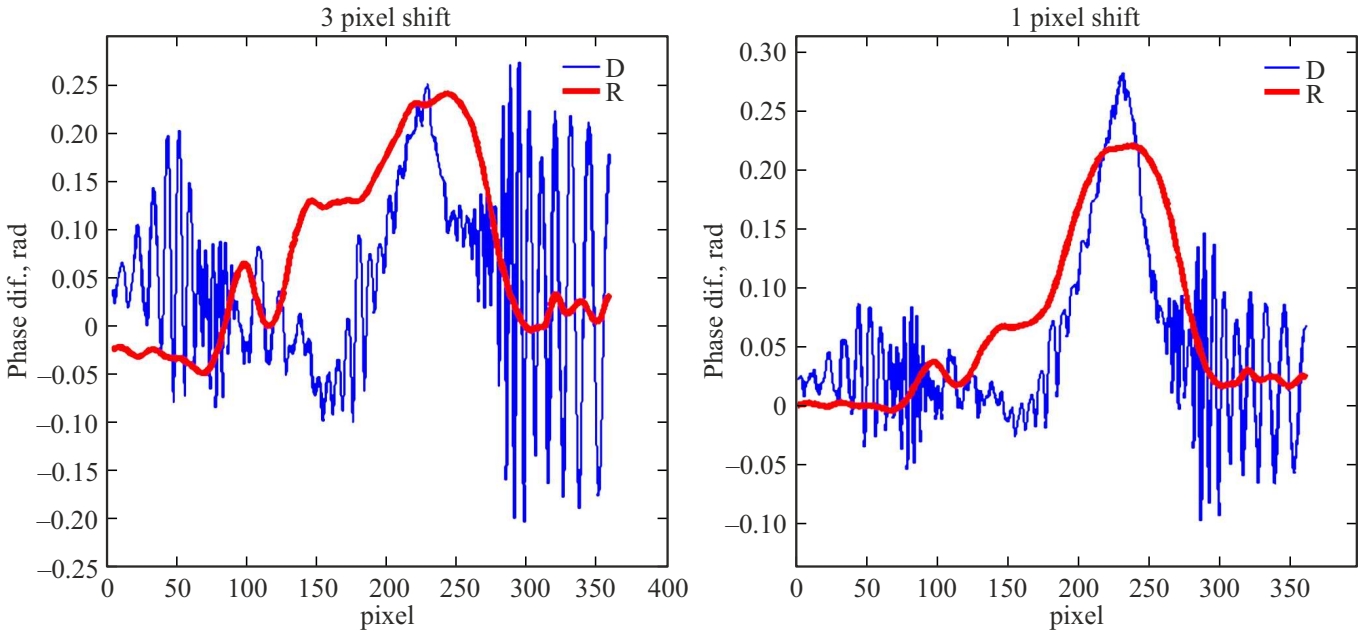

Figure 5. The difference between two distributions of reconstructed phases along the z axis, passing through the maximum of inhomogeneity, at various values of the amplitude of the Gaussian function of the cell model when shifting the object between calculations by 3 pixels in the object space. The red (thick) line — back projection (R), the blue (thin) line — back propagation (D) (*a*). The difference between two distributions of reconstructed phases along the z-axis passing through the maximum of inhomogeneity at various values of the amplitude of the Gaussian function of the cell model when shifting the object between calculations by 1 pixel in the object space. The red (thick) line — back projection (R), the blue (thin) line — back propagation (D) (*b*).

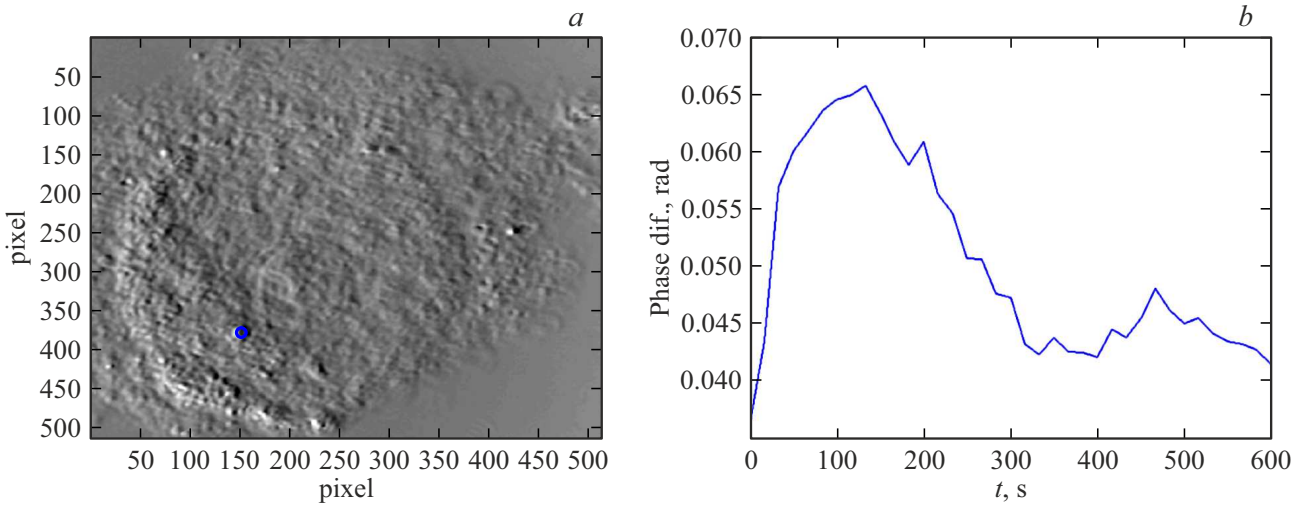

Figure 6. Differential projection obtained at $\varphi = 0$ for the initial tomogram of the leech Retzius neuron. The point of interest in the perinuclear region of the cell, where changes were observed, is circled (*a*). The time dependence of the phase change on the differential projection of the cell obtained at $\varphi = 0$ at the selected point of interest (*b*).

transformation procedure was performed on the obtained distributions. Denote the recovered refractive index dependencies on z at the point of interest x_{ROI}, y_{ROI} as $f^{\mathrm{ROI}}_{R,D}(z,t)$. Here ROI is the abbreviation from region of interest, lower indices R and D denote the corresponding algorithms — by Radon or by Devaney. Since normalizing values obtained by different algorithms is a non-trivial task, for convenience of comparing results, a data scaling procedure was performed according to the following formulas:

$$f_{\mathrm{R}}(z,t) = f^{\mathrm{ROI}}_{\mathrm{R}}(z,t),$$

$$f_{\mathrm{D}}(z,t) = a f^{\mathrm{ROI}}_{\mathrm{D}}(z,t) + b. \qquad (5)$$

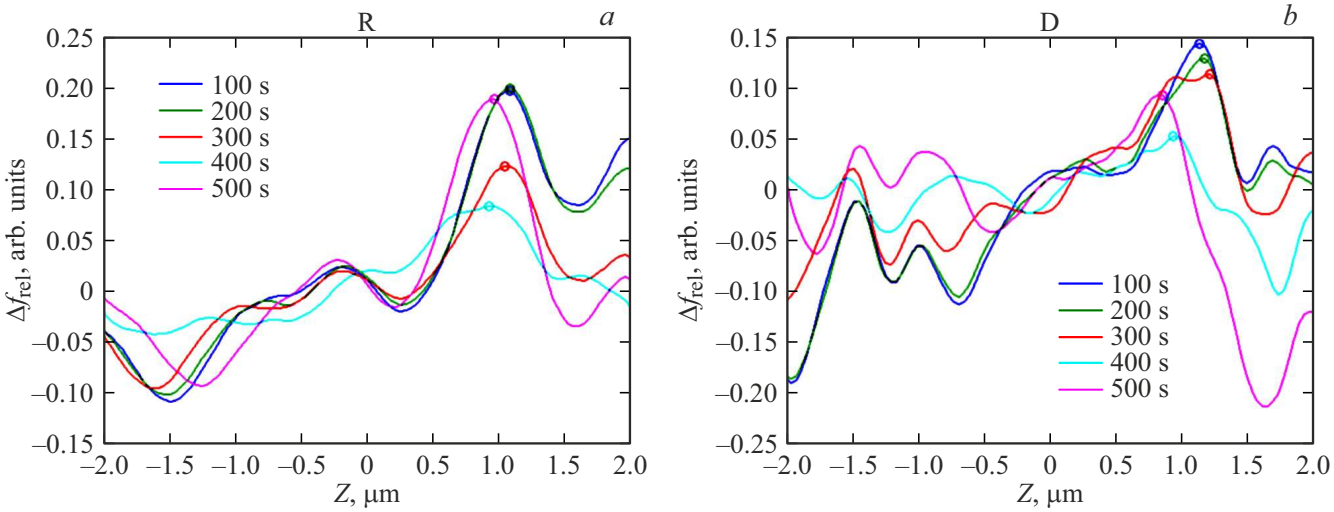

Figure 7. (a) Graphs depicting the reconstruction of the phase difference distribution along thee z axis at the point of interest using the back-projection method (R) for five distinct time points. (b) Corresponding graphs obtained via the back-propagation method (D).

Here the coefficients a, $b$in (5) were calculated using the formula

$$\min_{a,b}\Sigma_z (f_{\mathrm{R}}^{\mathrm{ROI}}(z,0) - a f_{\mathrm{D}}^{\mathrm{ROI}}(z,0) - b)^2.$$

Further analysis was conducted not on the recovered values themselves, but on their changes over time. For this purpose, quantities were calculated representing the deviation of changes in values relative to the initial time $t = 0$, normalized by the distribution along z at the initial time:

$$\Delta f_{\mathrm{R,D}}(z,t) = \frac{f_{\mathrm{R,D}}(z,t) - f_{\mathrm{R,D}(z,0)}}{f_{\mathrm{R,D}}(z,0)}.$$

On the resulting dependencies, sections along z without any features and sections where changes occur over time were clearly distinguished. Additionally, the graphs showed a slowly varying constant component over time, which should be attributed to low-frequency phase noise of the instrument. Therefore, for ease of comparison, constant components were subtracted from all dependencies $\Delta f_{\mathrm{R,D}}(z,t)$ calculated as averages over sections along z without features. For Radon reconstruction, this range was from -1.5 to $0.5\,\mu$m, and for Devaney reconstruction — from 0.5 to $0.5\,\mu$m. The obtained dependencies for several values of t are shown in the figures below.

Fig. 7, a shows the graphs corresponding to the recovery of the phase difference distribution along the axis z using the inverse projection method (R) for five different time points. Fig. 7, b shows similar graphs obtained using the backpropagation method (D).

Note that the processing results of experimental data match the modeling results (Fig. 4, a, 4, b, and Fig. 5). The time changes in phase differences for both inverse projection (Fig. 7, a) and backpropagation show the same trend (depending on the cell state). Evidently, during 10 min of cell receptor stimulation by the mediator (glutamate),

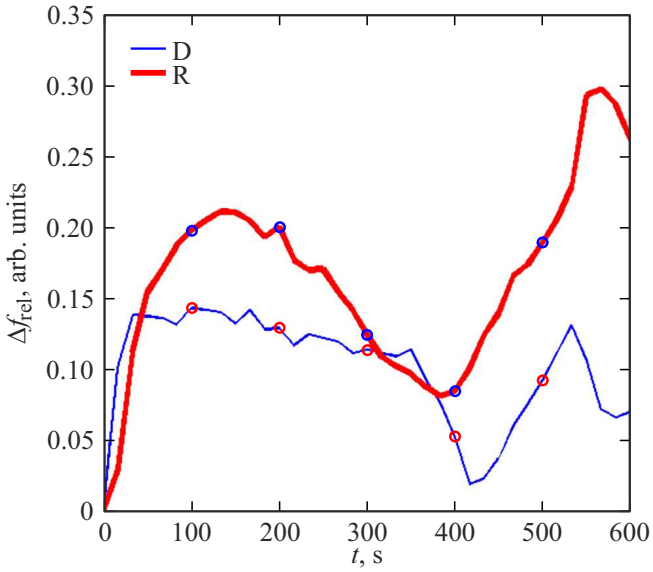

Figure 8. Density change Δf_{rel} in relative units versus time. Values f were taken at a point $z = 1\,\mu$m from the focusing line. Red (thick) line — inverse projection (R), blue (thin) line backpropagation (D).

microvesicle clusters in the cell cytoplasm shift outward, with almost no accompanying changes in the phase image. Therefore, secondary maxima appear on the graph of phase difference versus z. The phase difference on Fig. 7, a is smoother with a minimal number of secondary maxima. In Fig. 7, b, there are many maxima caused by micro-displacements of the object, making it difficult to identify the point of maximum changes. In Fig. 7, a, the point on the z axis with maximum phase difference changes corresponding to density changes inside the cell was selected; on Fig. 8, the density changeΔI versus time is

shown. Values were taken at a point $Z = 1\,\mu$m from the focusing line.

Note that the appearance of both curves differs little from each other, as in modeling (Fig. 4, *c*), indicating that the results of recovering density changes inside the cell at the selected point using backpropagation and inverse projection algorithms practically coincide. Comparison with the time variation of the measured phase at the point of interest selected on the projection obtained at $\varphi = 0$ (Fig. 6, *b*) shows that the local density change inside the cell under glutamate action at a depth of $1\,\mu$m from the focusing plane almost completely determines the transformation of its phase image. Thus, the proposed algorithm allows determining the coordinates of the organelle inside the cell most sensitive to external influence.

Conclusion

This study is devoted to developing a new method for analyzing intracellular dynamics of biological objects whose size exceeds the microtome field of view and whose internal structure reconstruction is impossible. This task is highly relevant for studying the dynamics of large single cells and cellular structures, as it enables analyzing which cell organelles are most sensitive to external stimuli.

Optical radiation propagation in such structures is described not by the eikonal equation, but by diffraction equations at least in the Born approximation. Therefore, localizing the region of structure change inside the cell required, on one hand, developing the LDT method and studying it via mathematical modeling, and on the other, developing an algorithm to determine the coordinates of this region.

Mathematical modeling of the local reconstruction process and experimental validation showed that the developed algorithms for processing diffraction projections allow determining coordinates of local density changes inside the cell even when its size significantly exceeds the microobjective field of view. It should be noted that the increased sensitivity of reconstruction to micro-displacements of the object between exposures prevents determining density change coordinates inside the cell using the backpropagation algorithm (Devaney). Meanwhile, local reconstruction by the inverse projection algorithm (Radon) successfully solves this task. Modeling showed that local projection (Radon) and local propagation (Devaney) reliably detect the qualitative dependence of local changes at the point of interest in the reconstructed distribution on refractive index changes inside the model. However, quantitative relations substantially depend on the number of projections, probing angle, and probing area size.

The proposed algorithms were used to process projection data of a real object leech Retzius neuron — under neurotransmitter influence. Experimental results showed good agreement with the simulation results. Notably, the inverse projection algorithm (Radon) for differential projections measured in our tomograph allows more confidently determining the density change region inside the cell. This is apparently due to object micro-displacements, which enhance diffraction effects when using the backpropagation algorithm (Devaney). Experiments showed that the dynamics of density change processes are reliably determined by local algorithms, but the question of their quantitative relations remains open. Solving this will require prior information about processes occurring in the cell.

Conflict of interest

The authors declare that they have no conflict of interest.

References

[1] G.N. Vishnyakov, G.G. Levin. Opt. Spectrosc., **85**, 73 (1998).
[2] C.G. Pack. Biophysics and Physicobiology, **18**, 244 (2021).
[3] K. Kim K. et al. Optics express, **21** (26), 32269 (2013).
[4] G. Kim et al. Scientific Reports, **8** (1), 9192 (2018).
[5] C. Zuo et al. Optics and Lasers in Engineering, **128**, 106003 (2020).
[6] A.J. Lee et al. Biomedical Optics Express, **12** (11), 6928 (2021).
[7] G.N. Vishnyakov, G.G. Levin, V.L. Minaev, V.V. Pickalov, A.V. Likhachev. Microscopy and Analysis, **18** (1), 19 (2004).
[8] R. Clackdoyle, M. Defrise. IEEE Signal Processing Magazine, **27** (4), 60(2010).
[9] A.G. Ramm, A.I. Katsevich. *The Radon Transform and Local Tomography*, 1st ed. (CRC Press, Boca Raton,1996).
[10] G.N. Vishnyakov, G.G. Levin, V.L. Minaev, N.A. Nekrasov. Opt. i spektr., **121** (6), 1020 (2016) (in Russian).
[11] E. Wolf. Opt. Commun., **1** (4), 153 (1969).
[12] A.J. Devaney. Ultrasonic Imaging, **4** (4), 1982, 336 (1982). DOI: 10.1016/0161-7346(82)90017-7
[13] G.G. Levin. *Sposob opredeleniya koordinat izmeneniya struktury kletki po fazovym izobrazheniyam*, patent RU 2761480 C1 (application 15.02.2021; published on 08.12.2021).
[14] B.A. Fihman. Mikrobiologicheskaya refraktometriya (Medicina, M., 1967). (in Russian)
[15] V.Ya. Brodskij, N.V. Nechaeva. *Ritm sinteza belka* (Nauka, M., 1988). (in Russian)
[16] A. Kuś et al. J. Biomed. Optics, **19** (4), 046009 (2014).
[17] G.G. Levin, A.A. Samojlenko., T.A. Kazakova, T.A. Marakuca, G.V. Maksimov. Biofizika, **68** (1), 57 (2023). (in Russian).
[18] G.N. Vishnyakov, G.G. Levin, V.L. Minaev, M.I. Latushko, N.A. Nekrasov, V.V. Pickalov. Optics Letters, **41** (13), 3037 (2016). DOI: 10.1364/OL.41.003037
[19] G.N. Vishnyakov, G.G. Levin, V.L. Minaev, M.M. Ermakov. Opt. i spektr., **125** (12), 864 (2018) (in Russian).

Translated by J.Savelyeva